

Freak waves in the linear regime: A microwave study

R. Höhmann¹, U. Kuhl¹, H.-J. Stöckmann¹, L. Kaplan², and E. J. Heller³

¹*Fachbereich Physik der Philipps-Universität Marburg, D-35032 Marburg, Germany*

²*Department of Physics, Tulane University, New Orleans, Louisiana 70118, USA*

³*Department of Physics and Department of Chemistry and Chemical Biology, Harvard University, Cambridge, Massachusetts 02138, USA*

(Dated: March 21, 2019)

Microwave transport experiments have been performed in a quasi-two-dimensional resonator with randomly distributed scatterers, each mimicking an r^{-2} repulsive potential. Analysis of both stationary wave fields and transient transport shows large deviations from Rayleigh's law for the wave height distribution, which can only partially be described by existing multiple-scattering theories. At high frequencies, the flow shows branching structures similar to those observed previously in stationary imaging of electron flow. Semiclassical simulations confirm that caustics in the ray dynamics are likely to be responsible for the observed structures. Particular conspicuous features observed in the stationary patterns are "hot spots" with intensities far beyond those expected in a random wave field. Reinterpreting the flow patterns as ocean waves in the presence of spatially varying currents or depth variations in the sea floor, the branches and hot spots lead to enhanced frequency of freak or rogue wave formation in these regions.

PACS numbers: 42.25.Dd, 05.45.Mt, 42.25.Bs

Scanning tunneling microscopy studies of electron flow through a high-mobility two-dimensional electron gas (2DEG) by Topinka et al. [1] exhibited intricate branching patterns of fractal appearance. This behavior was in contrast to the simple random wave prediction for the probability distribution of wave heights $|\Psi|$: $p_{\text{Rayleigh}}(I) = e^{-I}$, where $I = |\Psi|^2$ is proportional to the wave intensity, and the average value of I is 1. It was shown by Topinka et al. that the evolution of caustics (singularities of the ray density) in a correlated random potential is responsible for the formation of these branches, and later shown by Kaplan that the probability distribution of the branches may be computed analytically if the strength and correlation length of the random potential are known [2]. The phenomenology is not restricted to the flow of electrons through a disordered two-dimensional potential, but should hold equally well, e. g., for the propagation of light through a medium with varying index of refraction, resulting in the twinkling of starlight [3], or the evolution of wave patterns in the sea due to local variations in the surface current. The effect of eddy currents on an incoming sea has been studied by Heller et al. [4], who showed that even after accounting for dispersion in wavelength and direction, random currents cause large amplitude events to become much more common; they argued that such events might act as a trigger for non-linear instability effects in freak wave formation.

Motivated primarily by the experiments by Topinka et al., we undertook a microwave experiment to study the transport of waves through an arrangement of randomly distributed scatterers. Figure 1 shows a photograph of the experimental setup. The metallic bottom plate supports the scattering arrangements made up of about 55 to 60 brass cones. The source antenna is mounted close



FIG. 1: (Color online) Photograph of the set-up for one of the two scattering arrangements used. The platform has width 260 mm and length 360 mm. Each cone has diameter 25 mm and height 15 mm. The probe antenna is fixed in a top plate located 20 mm above the bottom (not shown) and can be scanned in two horizontal dimensions to map the field distribution within the scattering arrangement.

to one of the short sides, and its position can be varied, thus enabling the incoming waves to arrive from different directions. The drain antenna is mounted in the top plate (not shown), and acts as a weak probe. The top plate can be moved in both horizontal directions, allowing for a spatial mapping of the wave fields within the scattering arrangement.

For quasi-two-dimensional systems with parallel top and bottom plates separated by a distance d , the electromagnetic wave equations reduce to a single, scalar equation for the perpendicular component $E_{\perp}(x, y, z)$ of the electric field. Furthermore, we can separate the z coordinate, $E_{\perp}(x, y, z) = E(x, y) \cos(n\pi z/d)$, where n is the transverse quantum number, resulting in a two-dimensional wave equation for $E(x, y)$,

$$\left[-\frac{\partial^2}{\partial x^2} - \frac{\partial^2}{\partial y^2} + \left(\frac{n\pi}{d} \right)^2 \right] E(x, y) = k^2 E(x, y). \quad (1)$$

The number of active modes depends on frequency. For $f < c/2d$ only the lowest mode, $n = 0$, is open, and

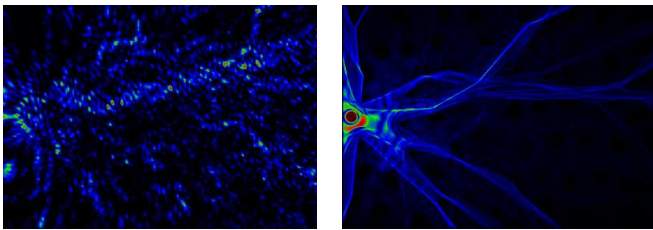


FIG. 2: (Color online) Comparison of an experimental wave pattern with a classical ray simulation. Left: A wave function for the frequency $f = 30.95$ GHz. Right: The corresponding semiclassical simulation, with modes 1 through 4 added together.

Eq. (1) is equivalent to the free stationary Schrödinger equation in the plane, where k^2 is proportional to the eigenenergy, and $E(x, y)$ to the wave function $\Psi(x, y)$ [5]. Eq. (1) remains approximately true when d varies with position, provided the variation is slow on the scale of the wave length. For $n > 0$, the additional term then mimics a potential, $V(x, y) = [n\pi/d(x, y)]^2$ [6]. For each cone in the experiment we obtain a repulsive central potential: $V(r) \propto (C + \min(r, r_0))^{-2}$, where $r_0 = 12.5$ mm is the cone radius and $C = 16.7$ mm is a constant determined by the cone geometry. At higher orders, however, the height variation will generate additional terms in Eq. (1) leading to a mixing among the modes.

The left panel of Fig. 2 shows a typical wave pattern observed for $f = 30$ to 40 GHz, the upper limit accessible by our equipment. At these frequencies, modes $n = 0$ to 4 are propagating. The corresponding wave lengths are between 7.5 and 10 mm, i. e., somewhat smaller than but comparable to the cone diameter and the mean distance between cones. In this open system, we observe exponential decay of the wave intensity with distance from the source caused by escape of the waves from the scattering setup as well as by absorption. This decay is suppressed in all plots. The right panel of Fig. 2 shows the results of a ray simulation, obtained by solving the classical equations of motion in the potential generated by the scatterers. The pattern bears a striking similarity with the branch-like structures found by Topinka et al. [1] in studies of 2DEG electron flow through quantum point contacts. The present results provide strong evidence in favor of the conjecture [1, 2] that correlated random potentials are responsible for these features.

To avoid the complication of mixing of up to five different modes, most of the experiments have been performed between 7.5 and 15 GHz, where only the first two modes $n = 0$ and 1 are propagating. In this regime, however, the wave lengths are large compared to the size of the scatterers, and interpretation of the cones in terms of a classical particle potential loses its justification. In fact, a measurement with a single cone shows that each cone scatters the waves isotropically with a cross-section of several mm depending slightly on frequency. Assuming

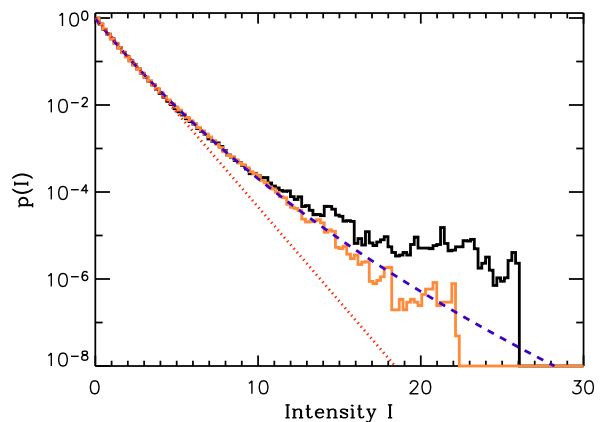


FIG. 3: (Color online) Probability distribution of intensities. The dark (black) histogram shows the distribution including all data, while the light (yellow) histogram excludes frequencies associated with the hot spot regions. The dotted line corresponds to the Rayleigh distribution, while the dashed (blue) line is a best fit using the theoretical distribution (2) ($\gamma \approx 23.5$).

single scattering, the resulting mean free path is 200 to 300 mm for our scatterer density, depending on frequency, and thus comparable to the system size; the real mean free path is slightly reduced due to multiple scattering.

There have been a number of wave transport studies in the weakly disordered regime, both theoretically and experimentally. Mirlin et al. [7] in particular gave explicit expressions for the transmission between two antennas embedded in a quasi-one-dimensional disordered sample,

$$p_{\text{dis}}(I) \approx \exp \left\{ -\frac{\gamma}{2} \left[\ln^2 \left(\sqrt{1 + \frac{2I}{\gamma}} + \sqrt{\frac{2I}{\gamma}} \right) \right] \right\}, \quad (2)$$

where γ is proportional to the conductance and depends also on the position of the two antennas. For $\gamma \gg I$, we have $p_{\text{pert}}(I) \approx e^{-I+2I^2/3\gamma}$, where the I^2 term gives the first perturbative correction to Rayleigh's law. Though our arrangement is not precisely in the quasi-one-dimensional limit, we still use Eq. (2) for our analysis, since it surely contains the generic leading correction for weak disorder. A related expression for the leading correction to Rayleigh had been given earlier by Nieuwenhuizen and van Rossum [8], and experimentally verified in a microwave transport experiment by Genack and Garcia for the case where both antennas are outside the sample [9]. We note that all corrections to Rayleigh contained in such multiple-scattering expressions are essentially finite wave length effects, disappearing in the limit of short wave length (high frequency or large γ). This is not the case with smooth potentials, which semiclassically deflect the flow; indeed the effect of classical caustics becomes more pronounced at short wave lengths [2].

Figure 3 shows the intensity distribution found in our experiments, averaged over a large data set (two scattering arrangements, three source antenna positions for

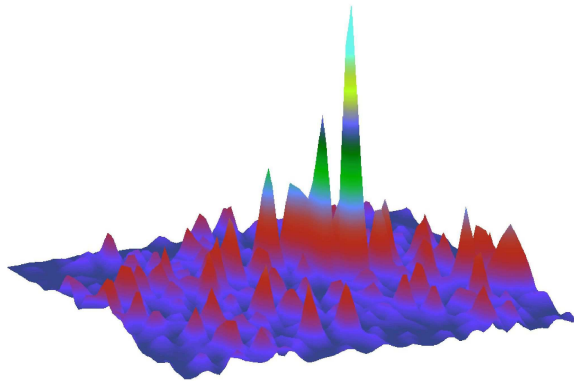


FIG. 4: (Color online) A “hot spot”, observed at a frequency of 8.85 GHz. The experimental probability density for observing such a hot spot is one to two orders of magnitude larger than expected from multiple scattering theory.

one of the arrangements, and a frequency range of 7.5 to 11 GHz). The distribution can be well described by Eq. (2) over three orders of magnitude, with γ as a free parameter. Here the situation is comparable to the one found by the Genack group in a number of studies [10]. But for the very high intensities, the probability exceeds by one to two orders of magnitude the expectation from multiple scattering theory.

Looking into the details, we find that there are just two regions (and another one at the border of significance) that are responsible for these deviations, one of them shown in Fig. 4. Each of these “hot spots” exists only in a limited frequency window about 500 MHz in width, and the range of incoming wave directions able to excite each hot spot is only about 20 degrees wide. If the frequency ranges containing these hot spots are omitted from the analysis, the resulting intensity distribution is in full agreement with the predictions from Eq. (2), see Fig. 3.

For the study of time-dependent waves, such as those found in the sea, we must superimpose waves with different frequencies, entering from different directions. To this end we concentrate on one hot spot found at 9.5 GHz near the center of our scattering arrangement. We vary the antenna position over 80 mm along the short side of the scattering arrangement (see Fig. 1), and record the resulting field pattern for each antenna position and each frequency. Then time-dependent wave fields are generated by superposition of $N = 150$ patterns,

$$\psi(\vec{r}, t) = \sum_{i=1}^N \psi_i(\vec{r}) e^{i(2\pi f_i t - \varphi_i)}. \quad (3)$$

Here $\psi_i(\vec{r})$ is a wave pattern at frequency f_i , excited with the source antenna at position x_i , and φ_i is a random phase. The randomly chosen frequencies f_i are normally distributed with the average at 9.5 GHz and a standard

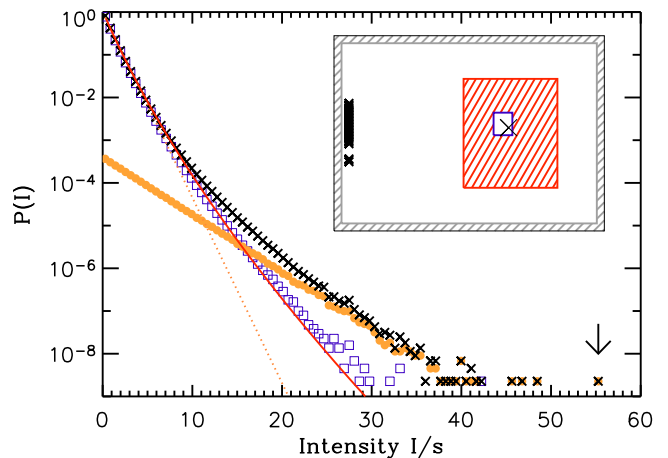


FIG. 5: (Color online) Intensity distribution for the time-dependent wave patterns generated by Eq. (3) for all measured points (dark (black) crosses), for points in the hot spot region only (light (orange) solid circles), and for all points excluding the hot spot (light (blue) open squares). The dotted line corresponds to the random wave expectation, while the solid (red) line is calculated using Eq. (7). The arrow indicates the pattern used for the time evolution study presented in Fig. 7. The inset shows a sketch of the set up. The dark crosses on the left of the inset mark the different exciting antenna positions, the (red) shaded region corresponds to the measured field, and the empty rectangle inside the measured field indicates the hot spot region. The cross inside the hot spot region is the position of the maximal measured intensity.

deviation of 0.764 GHz, thus covering approximately the frequency window in which this hot spot is present. Similarly, the antenna positions x_i are taken within the angle of acceptance of the hot spot.

Fixing the probe position, we always find a Rayleigh law for the distribution of intensities in a time sequence,

$$P_{\text{loc}}(I) = s^{-1} e^{-I/s} \quad (4)$$

but with the time-averaged value $s = \langle I \rangle$ depending on position. This is nothing but a manifestation of the central limit theorem. An example taken at the hot spot is given by the orange symbols in Fig. 5. This is the situation a ship experiences at a given position. If now the ship changes its position, or, alternatively, if the random currents change, a Rayleigh law with another s is found. The overall distribution of time-dependent intensities, collected over position and/or realization of the disorder, is then given by

$$P(I) = \int_0^{\infty} ds \frac{g(s)}{s} e^{-I/s} \quad (5)$$

where $g(s)$ is the probability density to find a particular value of the local time-averaged intensity s . The same distribution $P(I)$ would be obtained over very long times for a single ship, due to slow motion of the ship through

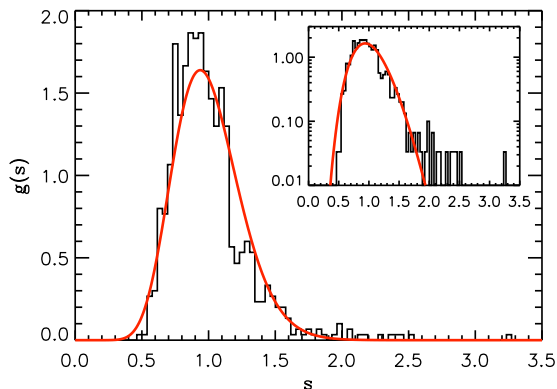


FIG. 6: (Color online) Distribution of the time-averaged intensities s found for the 780 pixels of our measurement. The inset shows the same data using a semi-logarithmic scale. The solid curve is a χ^2 -distribution with $\nu = 32$ degrees of freedom.

the random current field. A related approach was applied by Chabanov and Genack [11] to describe the probability distribution of microwave transmission intensities in disordered samples, but in the context of stationary patterns with no reference to time evolution.

Without loss of generality, we may take the average of s over position and/or disorder to be unity. We then find that $g(s)$ can be very well described by a chi-square distribution

$$g(s) = \chi_\nu^2(s) = \left(\frac{\nu}{2}\right)^{\frac{\nu}{2}} \frac{1}{\Gamma\left(\frac{\nu}{2}\right)} s^{\frac{\nu}{2}-1} \exp\left(-\frac{\nu s}{2}\right), \quad (6)$$

where the number of degrees of freedom ν is used as a fit parameter. This is exactly what is expected for a pulse made up of $\nu/2$ independent patterns obeying Rayleigh distributions. The number of degrees of freedom is independent of the total number of patterns N , but increases linearly both with the frequency range used, and the range of source antenna positions. A typical example is shown in Fig. 6. If the input patterns are not Rayleigh distributed but show the modified Rayleigh distribution (2) instead, a correspondingly modified χ^2 distribution is obtained. Taking into account the leading I^2 correction only, this can be done easily analytically. The corrections to expression (6) become significant in the range of high amplitudes.

With expression (6) for $g(s)$, the integral (5) can be performed analytically with the result

$$P(I) = \frac{1}{\Gamma\left(\frac{\nu}{2}\right)} \left(\frac{\nu I}{2}\right)^{\frac{\nu}{4}-\frac{1}{2}} K_{\frac{\nu}{2}-1}\left(2\sqrt{\frac{\nu I}{2}}\right), \quad (7)$$

where $K_\nu(x)$ is a modified Bessel function. The solid (red) line in Fig. 5 has been calculated from Eq. (7). It fits perfectly with the intensity distribution found if the spot region is excluded (blue squares), but not with the

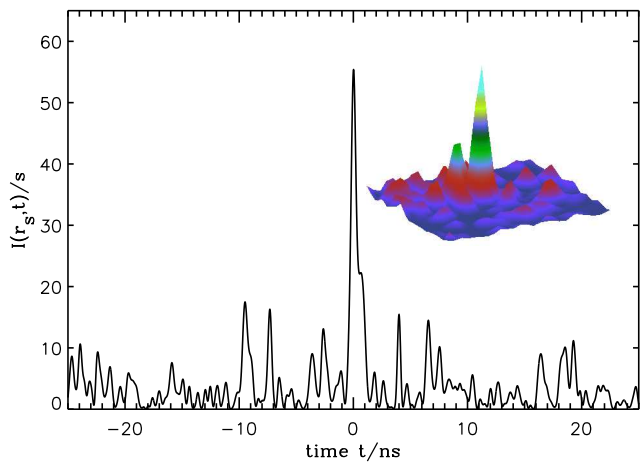


FIG. 7: (Color online) A freak wave event. The time evolution of wave intensity at the center of one of the hot spots is shown for the most extreme event observed. The inset shows the region surrounding the hot spot at the moment of the freak event. A movie of the time evolution in the entire field surrounding the hot spot is available [12].

distribution including the hot spot (black crosses). This is not really a surprise. Already the inset of Fig. 6 shows that the χ^2 distribution, though generally working very well, fails to describe the rare events in the high intensity tail.

Figure 7 shows the most extreme event found in our time series, marked by an arrow in Fig. 5, and the inset shows the entire region about the hot spot at the moment of this freak event. In the experiment, we observe events of this magnitude or greater with a probability of $1.3 \cdot 10^{-9}$. Thus, such events are still quite rare, but the probability is enhanced by 5 orders of magnitude compared with Eq. (7), and by 15 orders of magnitude compared to the Rayleigh distribution!

This work has demonstrated the virtues of microwave techniques for obtaining detailed information on wave transport through disordered surroundings. Simply by varying the frequency, we are able to study both ray dominated branching behavior of flow in a potential landscape, as well as the diffractive multiple scattering regime. The interpretation of the hot spots in this latter regime has to remain speculative for the moment, in view of the small number of such hot spots showing up in the experiments. However, the narrow angular acceptance of each hot spot, the visually obvious branching behavior at the higher frequencies, and particularly the fact that the observed deviations from Rayleigh statistics get stronger rather than weaker at shorter wavelengths, all support the hypothesis that ray refraction, as opposed to resonance, for example, is responsible for these extreme events. Perhaps the lasing modes found in random lasers [13] have their origin in similar hot spots.

-
- [1] M. A. Topinka, B. J. LeRoy, R. M. Westervelt, S. E. J. Shaw, R. Fleischmann, E. J. Heller, K. D. Maranowski, and A. C. Gossard, *Nature* **410**, 183 (2001).
- [2] L. Kaplan, *Phys. Rev. Lett.* **89**, 184103 (2002).
- [3] M. V. Berry, *J. Phys. A* **10**, 2061 (1977).
- [4] E. J. Heller, L. Kaplan, and A. Dahlen, *J. Geophys. Res.* **113**, C09023 (2008).
- [5] H.-J. Stöckmann, *Quantum Chaos - An Introduction* (University Press, Cambridge, 1999).
- [6] Y.-H. Kim, U. Kuhl, H.-J. Stöckmann, and J. P. Bird, *J. Phys.: Condens. Matter* **17**, L191 (2005).
- [7] A. D. Mirlin, R. Pnini, and B. Shapiro, *Phys. Rev. E* **57**, 6285(R) (1998).
- [8] T. M. Nieuwenhuizen and M. C. W. van Rossum, *Phys. Rev. Lett.* **74**, 2674 (1995).
- [9] A. Z. Genack and N. Garcia, *Europhys. Lett.* **21**, 753 (1993).
- [10] A. Z. Genack and A. A. Chabanov, *J. Phys. A* **38**, 10465 (2005).
- [11] A. A. Chabanov and A. Z. Genack, *Phys. Rev. E* **72**, 055602 (2005).
- [12] s. h. See EPAPS supplementary material at [URL will be inserted by AIP] for a movie showing a freak wave event. For more information on EPAPS.
- [13] H. Cao, Y. G. Zhao, S. T. Ho, E. W. Seelig, Q. H. Wang, and R. P. H. Chang, *Phys. Rev. Lett.* **82**, 2278 (1999).